
Localize-and-Stitch: Efficient Model Merging via Sparse Task Arithmetic

Yifei He^{1†} Yuzheng Hu¹ Yong Lin² Tong Zhang¹ Han Zhao^{1†}

¹University of Illinois Urbana-Champaign ²Hong Kong University of Science and Technology

Abstract

Model merging offers an effective strategy to combine the strengths of multiple finetuned models into a unified model that preserves the specialized capabilities of each. Existing methods merge models in a *global* manner, performing arithmetic operations across *all* model parameters. However, such global merging often leads to task interference, degrading the performance of the merged model. In this work, we introduce Localize-and-Stitch, a novel approach that merges models in a *localized* way. Our algorithm works in two steps: i) Localization: identify tiny (1% of the total parameters) localized regions in the finetuned models containing essential skills for the downstream tasks, and ii) Stitching: reintegrate only these essential regions back into the pretrained model for task synergy. We demonstrate that our approach effectively locates sparse regions responsible for finetuned performance, and the localized regions could be treated as compact and interpretable representations of the finetuned models (tasks). Empirically, we evaluate our method on various vision and language benchmarks, showing that it outperforms existing model merging methods under different data availability scenarios. Beyond strong empirical performance, our algorithm also facilitates model compression and preserves pretrained knowledge, enabling flexible and continual skill composition from multiple finetuned models with minimal storage and computational overhead. Our code is available at <https://github.com/yifei-he/Localize-and-Stitch>.

1 Introduction

Pretrained models [14, 38, 50, 49] contain a wealth of rich and generalizable information, and finetuning these models for specific downstream tasks significantly enhances performance compared to training from scratch [5]. With the growing popularity of the pretrain-finetune paradigm, a vast array of finetuned models have been made available on platforms like Hugging Face [63], and many of them originate from the same pretrained models, such as CLIP [49]. However, deploying multiple finetuned models independently, each for a different downstream task, incurs large storage and maintenance cost, and limits knowledge transfer across them.

Model merging offers a viable solution to these challenges by integrating the strengths of multiple finetuned models into a single model that retains the specialized capabilities of each. The key advantage of model merging over traditional multi-task learning (MTL) [3, 72, 29, 24] is its efficiency, in that it does not require joint training on data across all tasks, but only involves arithmetic operations in the weight space. Existing methods merge models by averaging model parameters via arithmetic mean [64, 30], Fisher information [40], regression mean [32] or learned merging weights [68]. Those methods all average the models in a *global* manner, meaning that they perform arithmetic operations to *all* parameters of the finetuned models. However, similar to the conflicting gradient problem in MTL [71, 37],

[†]Correspondence to: Yifei He <yifeihe3@illinois.edu>, Han Zhao <hanzhao@illinois.edu>.

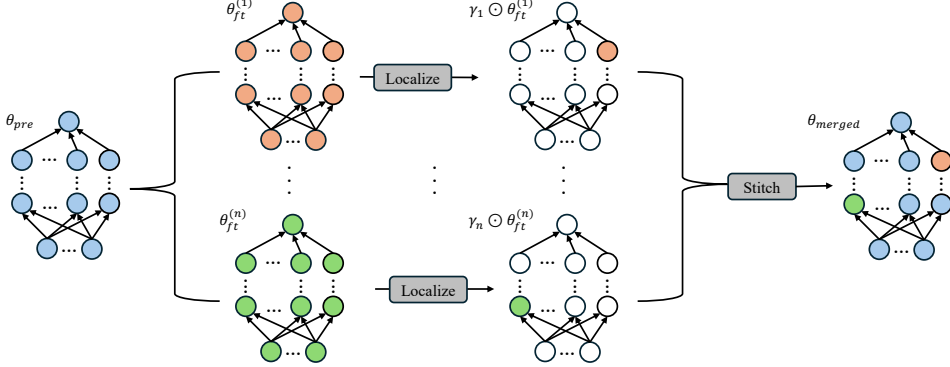


Figure 1: **Localize-and-Stitch**: Given n models $\{\theta_{ft}^{(i)}\}_{i=1}^n$ finetuned from θ_{pre} , we first localize regions containing skills acquired during finetuning through per-model binary masks $\{\gamma_i\}_{i=1}^n$, then stitch the localized regions $\{\gamma_i \odot \theta_{ft}^{(i)}\}_{i=1}^n$ onto the pretrained model, where \odot is the element-wise product. Empty nodes after the localization step mean that the mask is not activated at that position. Since the localized regions are tiny ($\sim 1\%$), we reduce potential task conflicts and make minimal changes to the pretrained model.

parameters in different finetuned models often have interference with each other, leading to suboptimal performance of the merged model. Recent works find that redundant parameter updates in finetuning are sources of conflicts [67]. Although the majority of model parameters are updated during finetuning, only very few contribute to improving the performance on downstream tasks [4, 27].

To overcome these limitations, we propose **Localize-and-Stitch**, an efficient algorithm that merges models in a *localized* manner. The algorithm (illustrated in Figure 1) involves two steps: i) Localization: identify tiny localized regions in the finetuned models containing essential skills for the downstream tasks. ii) Stitching: reintegrate only these essential regions back into the pretrained model. In the experiments, we verify that the changes in finetuned parameters are highly redundant, as we can efficiently identify just 1% of the total parameters that recovers over 99% of the finetuned performance. We evaluate our method on various language and vision tasks, showing that it outperforms existing model merging methods under different data availability scenarios.

Beyond the superior performance on model merging, our approach has several distinct advantages: i) Interpretability of task relations: each localized region encapsulates task-specific skills from the finetuned models, and overlap among them is indicative of knowledge sharing. ii) Model compression: Our localization method enables compact representation of finetuned models, significantly reducing the storage space to only 1% of the original without sacrificing performance. This enables flexible integration of finetuned models’ capabilities with minimal storage and computational overhead. iii) Preservation of pretrained knowledge: By making minimal and localized changes to the pretrained model, our merged model maintains its generalizability and achieves superior multi-task performance, effectively mitigating catastrophic forgetting associated with finetuning.

2 Preliminaries

Notation. Given a set of n tasks, we denote the pretrained model parameters as $\theta_{pre} \in \mathbb{R}^d$, the model parameters finetuned on the i -th task as $\theta_{ft}^{(i)} \in \mathbb{R}^d$. Note that all $\theta_{ft}^{(i)}$ are finetuned from the same pretrained model.

Task vectors. A task vector is the element-wise difference of the finetuned and pretrained parameters, denoted as $\tau_i = \theta_{ft}^{(i)} - \theta_{pre} \in \mathbb{R}^d$. These vectors encapsulate the knowledge acquired during the finetuning process. This knowledge can be effectively manipulated through task arithmetic [30], which involves performing arithmetic operations on task vectors to compose learned skills across tasks.

Model merging. The goal of model merging is to efficiently aggregate the parameters of the n finetuned models into a single multi-task model θ_{merged} without the need to retrain the model on the initial task-specific data. The resulting merged model should perform well on all the tasks simultaneously.

Existing methods perform merging in the general form $\theta_{merged} = \theta_{pre} + \sum_{i=1}^n \alpha_i \tau_i$, and their difference mainly lies in the way of determining the scaling factors α_i . We introduce the baselines in Table 1,

Table 1: Baselines for model merging.

Category	Method	Mathematical expression	Note
Global	Simple averaging [64]	$\theta_{\text{merged}} = \frac{1}{n} \sum_{i=1}^n \theta_{\text{ft}}^{(i)}$	Element-wise mean
	Task arithmetic [30]	$\theta_{\text{merged}} = \theta_{\text{pre}} + \alpha \sum_{i=1}^n \tau_i$	α tuned on a validation set
	Fisher merging [40]	$\theta_{\text{merged}} = \sum_{i=1}^n \hat{F}_i \theta_{\text{ft}}^{(i)} / \sum_{i=1}^n \hat{F}_i$	Weighted by Fisher information matrices
	RegMean [32]	$\theta_{\text{merged}} = (\sum_{i=1}^n X_i^\top X_i)^{-1} \sum_{i=1}^n (X_i^\top X_i \theta_{\text{ft}}^{(i)})$	Minimizes difference in merged and individual activations
Localized	AdaMerging [68]	$\{\theta_{\text{merged}}^l\}_{l=1}^L = \{\theta_{\text{pre}} + \sum_{i=1}^n \lambda_i^l \theta_{\text{ft}}^{(i)}\}_{l=1}^L$	Layer-wise weights learned by entropy minimization
	TIES-Merging [67]	Trims the parameters in task vectors with small magnitudes, elect a sign at each position of the task vector and only keep the parameters with the same sign.	

and categorize them into *global* and *localized* methods based on whether the algorithm incorporates selection strategies to identify which parameters to merge. Localized algorithms specifically target sparse and localized regions, while global algorithms merge parameters indiscriminately. Note that AdaMerging has two variants: one learns layer-wise weights and another learns task-wise weights. In this work, we refer to AdaMerging as the layer-wise version because of its superior performance over its task-wise counterpart.

Data requirements. Fisher merging [40] requires over 256 data points per task to estimate the Fisher information. RegMean [32] requires more than 1600 data points per task to compute the inner product matrices effectively. AdaMerging [68] needs access to the full unlabeled test set for entropy minimization. In contrast, simple averaging [64], task arithmetic [30] and TIES-Merging [67] can be implemented without additional data. However, to achieve the best performance, both task arithmetic and TIES-Merging require tuning the hyperparameter α on a validation set.

3 Localize-and-Stitch

We now introduce our main algorithm. In Section 3.1, we start by outlining two insights that underpin effective model merging, accompanied by motivating examples. In Section 3.2 and Section 3.3, we provide a detailed description of two key components of the algorithm: localization and stitching.

3.1 Motivation and objectives

Sparsity is important, but how to locate sparse regions is the key. Previous research identifies that during the finetuning stage, a significant portion of parameter updates is redundant, introducing interference in model merging [67]. This underscores the need for locating sparse regions to reduce such interference. While the importance of sparsity is recognized, strategies for achieving it remain underexplored. Earlier approaches typically identify sparse regions through random selection [70] or selecting regions with the top- $k\%$ largest magnitudes in task vectors [67]. However, they often fall short in identifying the most effective sparse regions for model merging. In Figure 2, we evaluate the efficacy of different localization methods across twelve language tasks, comparing the quality of their localized regions (specified by the binary mask γ_i). The performance is assessed on individual grafted models for each task, denoted as $\theta_{\text{pre}} + \gamma_i \odot \tau_i$, where τ_i is the task vector of the i -th task and \odot is the element-wise product. This grafted performance measures how well the finetuned skills are preserved when only keeping parameter updates during finetuning in localized regions. Unlike previous methods, we directly optimize the binary masks to maximally retain finetuned performance, detailed in Section 3.2. Our method significantly outperforms others, especially at lower sparsity levels. The strength of our approach lies in its precision in identifying small but informative regions, which is particularly advantageous for model merging.

Sparse regions with less overlap reduce task conflicts. Identifying the smallest possible regions with essential finetuned skills is key to minimizing potential conflicts among task vectors, as smaller localized regions naturally incur less overlap among tasks. With reduced overlap, each task can occupy its own, relatively disjoint localized region, thereby reducing task conflicts. This has the intuitive explanation that when two conflicting tasks share highly overlapping localized regions, they will compete to steer the parameters within these regions to their advantage in the merged model, leading to performance degradation. We demonstrate this by a case study (Figure 3) on merging models finetuned on two conflicting language tasks: QNLI [59] and MNLI [2]. QNLI involves predicting whether a context contains the answer to the given question, and MNLI involves predicting text entailment given a sentence pair. These tasks are conflicting, manifested by a noticeable performance

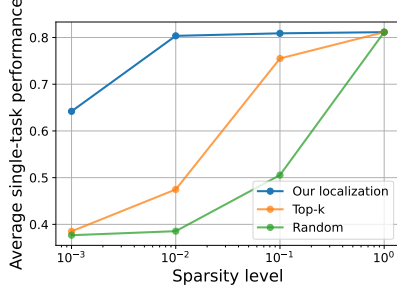


Figure 2: **Our method most effectively locates sparse regions essential for finetuned performance.** Sparsity level indicates the proportion of total parameters localized. By localizing only 1% of parameters (at sparsity level 0.01), our approach recovers 99% of the finetuned performance (at sparsity level 1).

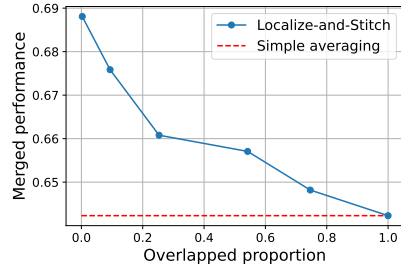


Figure 3: **Merged models with more parameter overlap manifest more task conflicts, resulting in performance decrease.** The overlapped proportion is over the model’s total parameter count. The simple averaging baseline is over all model parameters.

decline for both tasks when using simple averaging to merge the corresponding finetuned models. However, if the localized regions are small yet sufficiently informative about their respective tasks, the reduced overlap between these regions decreases task conflicts and enhances overall performance after merging. In other words, as long as the localized region contains sufficient task-specific knowledge, including more parameters than necessary in them only introduces additional task interference.

3.2 Localization

Motivated by the importance of locating informative yet small sparse regions, we outline two objectives for localization in finetuned models: i) the regions should encapsulate essential skills acquired during finetuning, and ii) they should contain minimal number of parameters.

The objectives are grounded in the findings of [45], which demonstrates that skills developed during finetuning are localizable. Specifically, grafting a small subset of finetuned parameters onto the pretrained model can almost fully recover the performance of the finetuned model. Panigrahi et al. [45] propose the following optimization problem to identify the localized parameters, and we adapt it in the model merging setting. With the constraint on the sparsity level s , on the i -th task with the loss function ℓ_i and task vector τ_i , we optimize for a binary mask γ_i such that only adding up the masked portion of the task vector onto the pretrained model performs well on the i -th task

$$\gamma_i = \underset{\gamma \in \{0,1\}^d: \|\gamma\|_0 \leq s}{\operatorname{argmin}} \ell_i(\theta_{\text{pre}} + \gamma \odot \tau_i),$$

where \odot denotes the element-wise product. For the ease of optimization, we follow [45] to reparametrize the binary mask γ as a real-valued vector S . To control the sparsity, we additionally relax the L_0 sparsity constraint to be L_1 . As a result, the optimization is reformulated as

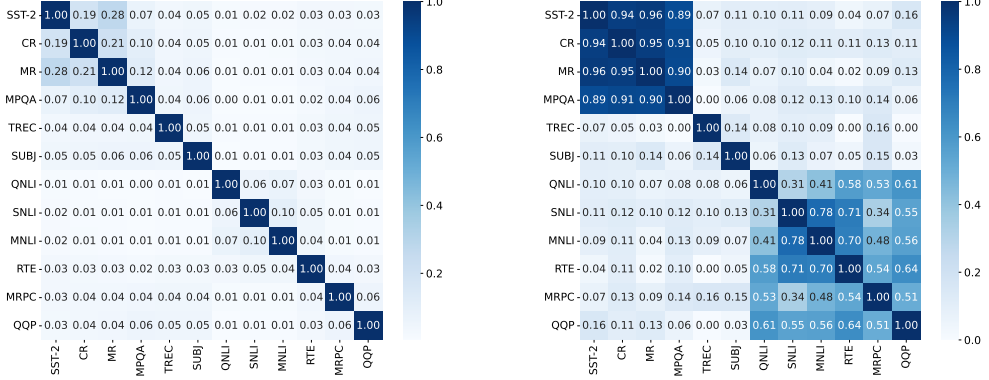
$$S_i = \underset{S \in \mathbb{R}^d}{\operatorname{argmin}} \ell_i(\theta_{\text{pre}} + \sigma(S) \odot \tau_i) + \lambda \|\sigma(S)\|_1, \quad (1)$$

Algorithm 1 Localize-and-Stitch

```

Input: Pretrained model  $\theta_{\text{pre}}$ , finetuned models  $\{\theta_{\text{ft}}^{(i)}\}_{i=1}^n$ , regularization coefficient  $\lambda$ , magnitude threshold  $k$ 
Output: Merged model  $\theta_{\text{merged}}$ , binary masks  $\{\gamma_i\}_{i=1}^n$ 
// Step 1: Localization
for  $i = 1, 2, \dots, n$  do
    Compute the task vector  $\tau_i = \theta_{\text{ft}}^{(i)} - \theta_{\text{pre}}$ 
    if validation data available then
         $S_i = \operatorname{argmin}_S \ell_i(\theta_{\text{pre}} + \sigma(S) \odot \tau_i) + \lambda \|\sigma(S)\|_1$ 
        // make the mask binary
         $\gamma_i = \operatorname{round}(\sigma(S_i))$ 
    else
        // Dataless Localization
         $\gamma_i[|\tau_i| > \text{top-}k(|\tau_i|)] = 1$  otherwise 0
    end if
end for
// Step 2: Stitching
for  $i = 1, 2, \dots, n$  do
    for  $k = 1, 2, \dots, d$  do
        // take average for overlaps
         $\gamma'_i[k] = \gamma_i[k] / \left( \sum_{j=1}^n \gamma_j[k] \right)$ 
    end for
end for
return  $\theta_{\text{merged}} = \theta_{\text{pre}} + \sum_{i=1}^n (\gamma'_i \odot \tau_i)$ 

```



(a) Jaccard similarity of pairwise task masks.

(b) Cosine similarity of masked task vectors.

Figure 4: **Our localized regions (each task with 1% of total parameters) have little pairwise overlap, with the majority of Jaccard similarity below 5%.** The sentiment classification tasks (SST-2, CR, MR, MPQA) have relatively large overlap because they share similar skills in the overlapping regions, and we verify this by showing that they have high cosine similarity of masked task vectors.

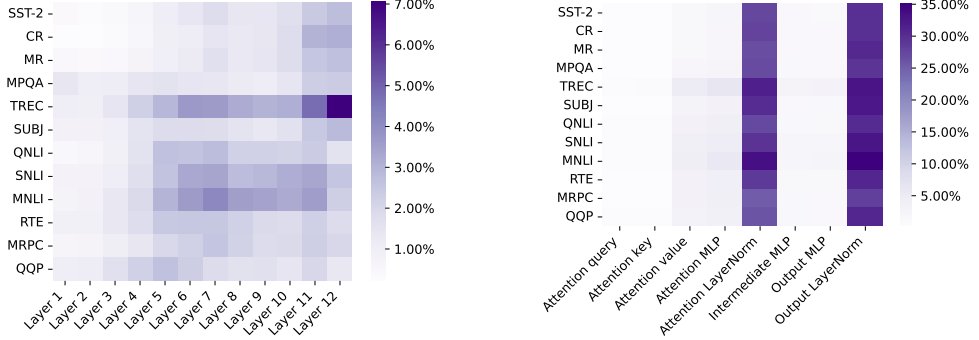
where σ is the sigmoid function, and λ controls the strength of the L_1 regularization. At the end of the optimization, we round $\sigma(S_i)$ to be binary. A detailed comparison between our localization technique and the one in [45] is presented in Appendix C. Note that the optimization is highly efficient, requiring as few as 8-shot data with 10 epochs of training using SGD. A detailed ablation on the impact of data availability on the mask quality is shown in Section 4.4.

Interpretation of task relationships. In Figure 4, we validate that our localization method effectively identifies task-specific regions with minimal overlap. In Figure 4a, we report the Jaccard similarity of all pairwise task masks, namely for each pair of masks γ_i and γ_j , we compute $|\gamma_i \cap \gamma_j| / |\gamma_i \cup \gamma_j|$. The majority of task pairs exhibit a Jaccard similarity below 5%, confirming minimal overlap. For the few pairs with Jaccard similarity larger than 10% (upper left corner of Figure 4a), we further compute the cosine similarity of their masked task vectors in Figure 4b, and find that their cosine similarities are almost 1, indicating high agreement of the parameters within the overlapped regions. Since these four tasks are all sentiment classification tasks, this phenomenon intuitively suggests a shared skill set across the tasks, located in the overlapped regions. We elaborate our resolution for the overlapped regions in Section 3.3

It is important to note that the meaningfulness of cosine similarity depends heavily on the presence of a substantial overlap, as indicated by Jaccard similarity. In cases where overlap is minimal, high cosine similarity might imply a strong relationship due to well-aligned parameters. Yet, this interpretation could be misleading without the broader context provided by Jaccard similarity, which could reveal that the actual interaction between the tasks is limited. This understanding is crucial for accurately assessing the nature of the relationships between tasks based on their localized parameters.

Distribution of localized regions. We analyze the distribution of the localized regions for language tasks in RoBERTa-base models Figure 5, both in terms of the layer index and the transformer components. For the layers, different tasks seem to occupy different layers, although the earlier layers in the network seldomly appear in the localized regions. Interestingly, most of the localized regions concentrate in the LayerNorm parameters. This pattern can possibly be attributed to a covariate shift observed in the finetuning data compared to the pretraining data, necessitating adjustments to the LayerNorm parameters to accommodate this shift. The same plots for GPT2-XL and ViT can be found in Appendix A, and the findings hold true for those models as well.

Localization without validation data. In the rare cases where no labeled data is available, we adopt a similar strategy as the “trim” step in TIES-Merging [67], which selects positions in task vectors with the top- $k\%$ largest magnitudes, i.e., the parameters changed the most during finetuning. We refer to our approach as **Dataless Localize-and-Stitch**. There are two key differences between **Dataless Localize-and-Stitch** and TIES: i) We find selecting the top-5% of parameters is sufficient for our pipeline, compared to the top-20% recommended by TIES-Merging. ii) We use Stitching described in the next section for merging the localized regions, instead of the “Elect”



(a) Distribution of localized regions in different network layers in the RoBERTa-base model. (b) Distribution of localized regions in different network components in the RoBERTa-base model.

Figure 5: **The localized regions are predominantly found in the LayerNorm parameters**, while different tasks are associated with different layers. The percentages represent the proportion of localized parameters in each component.

procedure in TIES. We detail the advantages of those design choices in Appendix B. As shown in Figure 2, to match the performance of localization with validation data, the dataless version typically requires locating larger regions. This expansion is necessary to encapsulate sufficient skills acquired during finetuning, but it also leads to increased task conflicts. Nevertheless, in Section 4, we show that our dataless version still outperforms all other methods that do not require additional validation data.

3.3 Stitching

After obtaining the binary mask for each task, we integrate these masks, and apply them to task vectors to construct the merged model. Given the sparsity, the masks generally activate different positions for different tasks, minimizing overlap. However, in instances where overlaps occur – that is, where multiple tasks share the same mask positions – we address this by averaging the parameters in these regions. Specifically, for each final mask γ'_i , the value at the k -th position, denoted $\gamma'_i[k]$, is calculated as the reciprocal of the total number of tasks that have a mask value of 1 at that position; if the original mask value $\gamma_i[k]$ is 0, it remains 0 in the processed mask

$$\gamma'_i[k] = \gamma_i[k] \Big/ \left(\sum_{j=1}^n \gamma_j[k] \right).$$

After we obtain the processed masks $\{\gamma'_i\}_{i=1}^n$, we apply them to the task vectors and stitch the masked task vectors to get the final merged model

$$\theta_{\text{merged}} = \theta_{\text{pre}} + \sum_i^n (\gamma'_i \odot \tau_i).$$

Note that our stitching step **does not involve tuning the scaling factors α** as other methods mentioned in Section 2, which typically requires grid search or other optimization strategies for tuning. This distinction simplifies our method and avoids the computational overhead. A comparison of runtime is provided in Appendix A.

Remark. In Localize-and-Stitch, the majority of computational overhead lies in the localization step, while the subsequent stitching process is notably efficient. This distribution of workload is ideal because the more intensive localization step is performed separately on each individual finetuned model. This property provides simple extension in continual learning settings: When integrating a new model into the existing merged model (or updating any of the merged models), only the localization step for that new model incurs a cost, followed by stitching. This is in contrast to most model merging methods [32, 30, 67, 68] which necessitate restarting the whole merging process, as the scaling factors of task vectors are tuned or learned based on the performance of the merged model. We provide an experiment of continual learning in Appendix A to illustrate this advantage.

Table 2: Multi-task performance of merged RoBERTa-base models on twelve NLP tasks.

Task	SST-2	CR	MR	MPQA	TREC	SUBJ	QNLI	SNLI	MNLI	RTE	MRPC	QQP	Average
Single-task finetuned	0.898	0.894	0.844	0.848	0.938	0.931	0.764	0.791	0.706	0.643	0.766	0.716	0.811
Simple averaging [64]	0.857	0.851	0.829	0.688	0.304	0.478	0.508	0.452	0.452	0.563	0.311	0.469	0.563
Task arithmetic [30]	0.846	0.856	0.769	0.810	0.156	0.584	0.607	0.538	0.403	0.539	0.822	0.581	0.626
TIES [67]	0.805	0.805	0.728	0.791	0.226	0.549	0.552	0.501	0.379	0.477	0.816	0.572	0.600
Dataless	0.909	0.907	0.864	0.821	0.462	0.762	0.558	0.690	0.618	0.688	0.837	0.693	0.734
Localize-and-Stitch													
Task arithmetic [30]	0.885	0.882	0.803	0.829	0.320	0.610	0.620	0.561	0.495	0.656	0.828	0.623	0.675
TIES [67]	0.886	0.88	0.852	0.835	0.226	0.482	0.548	0.359	0.397	0.594	0.794	0.603	0.621
Fisher merging [40]	0.900	0.898	0.837	0.758	0.260	0.546	0.542	0.725	0.652	0.656	0.833	0.677	0.690
RegMean [32]	0.897	0.897	0.847	0.826	0.730	0.791	0.559	0.683	0.568	0.638	0.794	0.642	0.739
AdaMerging [68]	0.850	0.861	0.778	0.815	0.230	0.595	0.612	0.541	0.404	0.547	0.822	0.588	0.637
Localize-and-Stitch	0.896	0.896	0.849	0.828	0.782	0.820	0.734	0.621	0.580	0.633	0.820	0.651	0.759

4 Experiments

We evaluate the performance of Localize-and-Stitch with baselines described in Section 2 under various experimental settings. Our localization step is performed with 64-shot validation data, and the sparsity is chosen to be 1%. In the dataless version, the sparsity is chosen to be 5%.

4.1 Merging finetuned encoder-based language models

Following Panigrahi et al. [45], we finetune the RoBERTa-base [38] model on twelve GLUE [59] tasks. Specifically, the dataset suite includes six single-sentence tasks (SST-2 [52], CR [28], MR [44], MPQA [61], TREC [58], SUBJ [43]) and six pairwise-sentence tasks (QNLI [59], SNLI [2], MNLI [62], RTE [59], MRPC [15], QQP [31]). The dataset details can be found in Appendix E.

We present the results in Table 2. The table is structured into three blocks for clarity: the upper block displays the performance of individually finetuned models for each task, the middle block lists algorithms that operate without the need for validation data, whereas the lower block includes algorithms that require validation data. Note that both the middle and lower blocks contain Task arithmetic and TIES because they are applicable with or without data. Both algorithms are able to utilize validation data to tune the merging coefficients α , as in $\theta_{\text{merged}} = \theta_{\text{pre}} + \alpha \sum_{i=1}^n \tau_i$. We follow common practice to search over $\{0.1, 0.2, \dots, 1\}$ to obtain the optimal coefficients. When no validation data is available, we use their suggested merging coefficient of 0.4.

From Table 2, regardless of data availability, our approach consistently outperforms other baselines. Notably, the dataless version of our algorithm provides more than 10% performance increase over task arithmetic and surpasses methods that depend on validation data (Fisher merging and AdaMerging), demonstrating its effectiveness. Note that TIES-Merging, although sharing one similar step with our dataless version, performs worse than task arithmetic. This performance decrease is also observed in similar language evaluation settings with similar model size [67]. We identify two possible factors for this phenomenon: i) the larger localized regions of TIES potentially lead to more task conflicts; ii) the sign election mechanism it employs tends to be less effective in overlapping regions that involve only a few tasks, particularly when just two are present. This can lead to suboptimal retention of essential task-specific information. We provide further analysis comparing Dataless Localize-and-Stitch and TIES-Merging in Appendix B.

4.2 Merging finetuned decoder-based language models

Compared with encoder-only language models, decoder-based language models benefit from increased number of parameters and perform well on complicated generative tasks. We use GPT2-XL [48] as the base model, and obtain three supervised finetuned checkpoints from the Hugging Face model hub [63], each tuned for distinct functionalities: general instruction following, scientific knowledge and truthfulness respectively. Further details about these models are specified in Appendix D.

To assess these models, we use MMLU [26], ARC [9] and TruthfulQA [36] as evaluation datasets for the respective domains. Unlike datasets in the previous section, these are typically used in their entirety for evaluation, without a designated train-test split. However, using these datasets for both evaluation and localization could lead to data leakage. To prevent this, we use data from three surrogate datasets with similar purposes for localization, namely Alpaca [56], GSM8K [10] and HotpotQA [69].

Table 3: Multi-task performance of merged GPT2-XL models on three evaluation benchmarks.

Task	MMLU	TruthfulQA	ARC	Average
Single-task	0.273	0.488	0.472	0.411
Simple averaging [64]	0.234	0.390	0.406	0.344
Task arithmetic [30]	0.234	0.390	0.399	0.341
TIES [67]	0.233	0.448	0.310	0.330
Dataless Localize-and-Stitch	0.256	0.394	0.427	0.359
Localize-and-Stitch	0.247	0.388	0.467	0.367

Table 4: Multi-task performance of merged CLIP ViT-B/32 models on eight vision tasks.

Task	SUN397	Cars	RESISC45	EuroSAT	SVHN	GTSRB	MNIST	DTD	Average
Single-task finetuned	0.753	0.777	0.961	0.997	0.975	0.987	0.997	0.794	0.905
Simple averaging [64]	0.653	0.634	0.714	0.717	0.642	0.528	0.875	0.501	0.658
Task arithmetic [30]	0.552	0.549	0.667	0.789	0.802	0.697	0.973	0.504	0.692
TIES [67]	0.598	0.586	0.707	0.797	0.862	0.721	0.983	0.542	0.725
Dataless Localize-and-Stitch	0.669	0.647	0.768	0.746	0.817	0.726	0.973	0.576	0.740
Task arithmetic [30]	0.638	0.621	0.720	0.776	0.744	0.651	0.970	0.522	0.701
TIES [67]	0.648	0.629	0.743	0.789	0.831	0.714	0.976	0.562	0.736
Fisher merging [40]	0.686	0.692	0.707	0.664	0.729	0.511	0.879	0.599	0.683
RegMean [32]	0.653	0.635	0.756	0.786	0.781	0.674	0.937	0.520	0.718
AdaMerging [68]	0.645	0.681	0.792	0.938	0.870	0.919	0.975	0.591	0.801
Localize-and-Stitch	0.672	0.683	0.818	0.894	0.879	0.866	0.948	0.629	0.799

We compare our approach with other methods directly applicable in this setting in Table 3. Both versions of Localize-and-Stitch noticeably outperforms other baselines. The result verifies that even for complex generative tasks, skills can still be localized within tiny regions of finetuned models. Moreover, this shows that good localization performance can be achieved without access to the original finetuning data; using similar data from other sources also suffices. This aligns with the finding from [45] that localized regions exhibit transfer among similar tasks, meaning that a localized region for one task can facilitate performance in related tasks. This further reduces the dependency on data availability, making our approach more versatile. Overall, these findings highlight the capability of Localize-and-Stitch to integrate the strengths from multiple language models, demonstrating its effectiveness across a variety of linguistic challenges.

4.3 Merging finetuned vision models

Following the practice in Ilharco et al. [30], we finetune the CLIP [49] image encoder with the ViT-B/32 [16] architecture on eight image classification tasks, incorporating diverse categories of images such as remote sensing, satellite images and traffic signs. Specifically, the dataset suite includes SUN397 [66], Stanford Cars [33], RESISC45 [6], EuroSAT [25], SVHN [41], GTSRB [53], MNIST [34] and DTD [8]. The details of each dataset can be found in Appendix E.

We present the results in Table 4. Similarly, even in the absense of validation data, the dataless version of our approach can outperform methods requiring validation data (Fisher merging and RegMean). When validation data is available, our method also demonstrates competitive performance. Note that AdaMerging, while achieving similar results as ours, imposes more demanding data availability requirement, and incurs higher computational cost. It necessitates entropy minimization across the entire (unlabeled) test set, rendering it approximately 15 times slower than our method.

4.4 Empirical analysis

Sparsity-performance trade-off. In the localization step, we optimize for two competing objectives: identifying regions containing sufficient finetuned skills, and minimizing the number of parameters involved. Here, we study the trade-off by presenting the performance of our approach on the language tasks at different sparsity levels in Figure 6. Across all models and tasks tested, we observe that a sparsity level around 1% yields the best results using our localization method, whereas dataless localization requires 5 – 10%. When the localized regions are too small to retain adequate finetuned knowledge, the benefit of less overlap is diminished. Conversely, when the localized regions are too large, although the regions possess sufficient finetuned knowledge, the increased overlap among task-specific regions leads to more task interference.

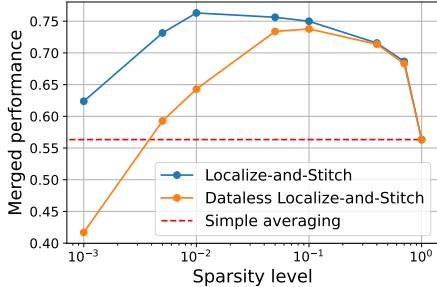


Figure 6: Sparsity-performance trade-off for our algorithm on the language tasks. Localization achieves the best performance at sparsity around 1%, while the dataless version requires 5–10%.

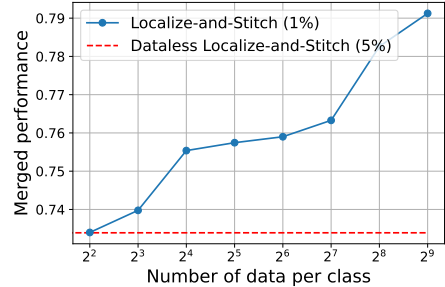


Figure 7: **With only 8-shot data, the performance of our algorithm improves over the dataless version.** With more data available, the performance of our method continues to increase. Numbers in brackets represent sparsity levels for each method.

Effect of data availability. We present the performance of our method across various data availability scenarios with a localization region of 1% (Figure 7) on the language tasks. One clear trend is that with more data, the quality of localization improves, resulting in enhanced performance of the merged model. Notably, even with as few as 8-shot data, the merged performance surpasses that of the dataless approach, highlighting its effectiveness under constrained data conditions.

Model compression through localization. Our localization approach enables a compact representation of the finetuned model. In our experiments, we find that localizing only 1% of the total parameters recovers over 99% of the performance achieved by single-task finetuning (full evaluation reported in Appendix A). The efficiency allows us to store only the masked task vectors for each task ($\gamma_i \odot \tau_i$) instead of the entire finetuned models, without a noticeable loss in performance. Given the sparsity of these masked task vectors, we can store them in Compressed Sparse Row (CSR) format [47, 19], which drastically reduces the model size to about 1% of the original. For example, a RoBERTa-base model, which typically requires $\sim 650\text{MB}$ of memory to store, can be represented using only a $\sim 7\text{MB}$ sparse matrix, achieving a memory reduction of 99%. Although we still need to store the full pretrained model, this storage overhead will be amortized with more finetuned models. This model compression, combined with the ease of update mentioned in Section 3.3, enables flexible composition of skills from multiple finetuned models with minimal storage and computational overhead.

Avoid forgetting of pretrained knowledge. Pretrained models contain rich and generalizable information, derived from their diverse training data. However, finetuning often incurs catastrophic forgetting of skills in the pretrained model [23, 39], which is carried over when these finetuned models are merged. As our method makes minimal change to the pretrained model, such forgetting is substantially mitigated. For instance, in the vision setting where we localize 1% parameters for each task, the total parameters changed in our merged model compared with the pretrained model is only around 7% for the 8 tasks as a result of minimal overlap. We evaluate the retention of pretrained capabilities with a general vision task that the pretrained model excels, namely zero-shot ImageNet classification [13], and report the results in Figure 8. Our method most effectively preserves the pretrained performance, while achieves superior performance on the eight merged tasks.

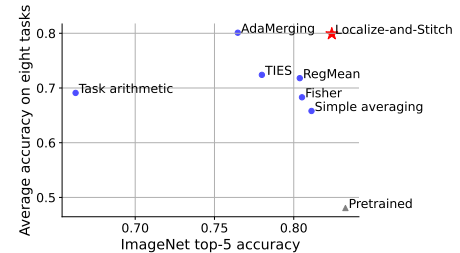


Figure 8: **Our method retains the pretrained skill the best** due to the minimal updates (7% of total parameters) to the pretrained model, while performs well on the eight merged tasks (upper right better).

CLIP model excels, namely zero-shot ImageNet classification [13], and report the results in Figure 8. Our method most effectively preserves the pretrained performance, while achieves superior performance on the eight merged tasks.

5 Related works

Model merging. Model merging aims at efficiently integrating multiple finetuned models into a single model that retains the capabilities of each. It is a promising solution to enhance the generalization and multi-task capabilities of finetuned models. Wortsman et al. [65, 64] demonstrates that merging models trained on the same task with different training configurations can improve the

out-of-distribution (OOD) robustness. Merging finetuned models from related tasks can provide an improved initialization for new tasks [7, 20]. Additionally, finetuned models with different specialized capabilities can be merged together for enhanced multi-task capabilities [30, 67, 40, 32, 68, 70, 60]. In this work, we primarily focus on merging model for enhancing multi-task performance. Similar to the gradient conflict problem [71, 37] in multi-task learning, finetuned models also manifest conflict when merged together, and our method provides an effective solution to this problem.

Our approach stands out with four key advantages: i) Localized merging: Instead of global merging, we localize merging to specific regions with finetuned skills, effectively decreasing task conflicts. ii) Simplified process: Existing works often require computationally intensive grid search or optimization to determine the optimal merging coefficients, while our stitching procedure does not have the requirement. iii) Data flexibility: Our method works with or without validation data, and provides competitive results in various data availability scenarios. iv) Benefits beyond model merging: This includes interpretability of task relations, model compression and preservation of pretrained knowledge.

Knowledge attribution. Recent works find that knowledge contained in language models is localizable, meaning that model behavior can be attributed to small subsets of model parameters. One line of work identifies such regions to edit the knowledge contained in the networks. Sundararajan et al. [55] uses integrated gradients for knowledge attribution, which measures how sensitive each neuron’s gradient is to the change of input. Dai et al. [12] applies integrated gradients to edit factual knowledge contained in BERT models. However, the relationship between the editing success and the localized regions remains unclear [22]. Another line of work aims at pruning large models. Lee et al. [35] proposes SNIP score, which computes the change of loss when each neuron is set to 0. Sun et al. [54] proposes Wanda score to optimize for a binary mask such that the masked activations is close to the original ones. Knowledge attribution can also be applied for enhancing interpretability. Vig et al. [57] applies causal mediation analysis [46] to identify individual neurons contributing to gender bias.

Recently, Panigrahi et al. [45] optimizes for a binary mask to localize the skills contained in finetuned language models and study task relationship based on it. There are two key differences between our localization formulation and theirs. Firstly, our formulation of S is more straightforward, as we directly have $\gamma = \sigma(S)$ in Equation (1). In contrast, Panigrahi et al. [45] uses S as a selector of whether to take the value from the initial mask, leading to more complex computation. Secondly, our approach uses the L_1 constraint to control the sparsity in a more fine-grained manner, while Panigrahi et al. [45] does not have this constraint, and controls sparsity via early stopping. We empirically show that our localization formulation identifies regions with improved quality in Appendix C.

6 Conclusion

In this work, we study the problem of task interference in the context of model merging. We find that globally merging models typically leads to task interference, due to the parameter redundancy in task vectors. To tackle this challenge, we introduce `Localize-and-Stitch`, which performs localized merging via sparse task arithmetic. We first identify tiny regions in the finetuned models that contain essential skills acquired during finetuning, and stitch only those regions back onto the pretrained model. Empirical evaluation on various vision and language benchmarks validate the effectiveness of our approach. Beyond model merging, our approach performs effective model compression, which compresses the model size to be 1% of the original without sacrificing performance. Additionally, `Localize-and-Stitch` also excels at retaining the pretrained knowledge. Overall, our approach offers a novel pathway for flexible and continual skills composition from finetuned models with minimal storage and computational overhead.

Acknowledgments and Disclosure of Funding

Han Zhao and Tong Zhang are partially supported by an NSF IIS grant No. 2416897. Han Zhao would also like to thank the support from a Google Research Scholar Award. Yifei He and Yuzheng Hu are partially supported by a research grant from the Amazon-Illinois Center on AI for Interactive Conversational Experiences (AICE). The views and conclusions expressed in this paper are solely those of the authors and do not necessarily reflect the official policies or positions of the supporting companies and government agencies.

References

- [1] Luisa Bentivogli, Peter Clark, Ido Dagan, and Danilo Giampiccolo. The fifth pascal recognizing textual entailment challenge. *TAC*, 7(8):1, 2009.
- [2] Samuel R Bowman, Gabor Angeli, Christopher Potts, and Christopher D Manning. A large annotated corpus for learning natural language inference. *arXiv preprint arXiv:1508.05326*, 2015.
- [3] Rich Caruana. Multitask learning. *Machine learning*, 28:41–75, 1997.
- [4] Tianlong Chen, Jonathan Frankle, Shiyu Chang, Sijia Liu, Yang Zhang, Zhangyang Wang, and Michael Carbin. The lottery ticket hypothesis for pre-trained bert networks. *Advances in neural information processing systems*, 33:15834–15846, 2020.
- [5] Ting Chen, Simon Kornblith, Mohammad Norouzi, and Geoffrey Hinton. A simple framework for contrastive learning of visual representations. In *International conference on machine learning*, pages 1597–1607. PMLR, 2020.
- [6] Gong Cheng, Junwei Han, and Xiaoqiang Lu. Remote sensing image scene classification: Benchmark and state of the art. *Proceedings of the IEEE*, 105(10):1865–1883, 2017.
- [7] Leshem Choshen, Elad Venezian, Noam Slonim, and Yoav Katz. Fusing finetuned models for better pretraining. *arXiv preprint arXiv:2204.03044*, 2022.
- [8] Mircea Cimpoi, Subhransu Maji, Iasonas Kokkinos, Sammy Mohamed, and Andrea Vedaldi. Describing textures in the wild. In *Proceedings of the IEEE conference on computer vision and pattern recognition*, pages 3606–3613, 2014.
- [9] Peter Clark, Isaac Cowhey, Oren Etzioni, Tushar Khot, Ashish Sabharwal, Carissa Schoenick, and Oyvind Tafjord. Think you have solved question answering? try arc, the ai2 reasoning challenge. *arXiv preprint arXiv:1803.05457*, 2018.
- [10] Karl Cobbe, Vineet Kosaraju, Mohammad Bavarian, Mark Chen, Heewoo Jun, Lukasz Kaiser, Matthias Plappert, Jerry Tworek, Jacob Hilton, Reiichiro Nakano, et al. Training verifiers to solve math word problems. *arXiv preprint arXiv:2110.14168*, 2021.
- [11] Ido Dagan, Oren Glickman, and Bernardo Magnini. The pascal recognising textual entailment challenge. In *Machine learning challenges workshop*, pages 177–190. Springer, 2005.
- [12] Damai Dai, Li Dong, Yaru Hao, Zhifang Sui, Baobao Chang, and Furu Wei. Knowledge neurons in pretrained transformers. *arXiv preprint arXiv:2104.08696*, 2021.
- [13] Jia Deng, Wei Dong, Richard Socher, Li-Jia Li, Kai Li, and Li Fei-Fei. Imagenet: A large-scale hierarchical image database. In *2009 IEEE conference on computer vision and pattern recognition*, pages 248–255. Ieee, 2009.
- [14] Jacob Devlin, Ming-Wei Chang, Kenton Lee, and Kristina Toutanova. Bert: Pre-training of deep bidirectional transformers for language understanding. *arXiv preprint arXiv:1810.04805*, 2018.
- [15] Bill Dolan and Chris Brockett. Automatically constructing a corpus of sentential paraphrases. In *Third international workshop on paraphrasing (IWP2005)*, 2005.
- [16] Alexey Dosovitskiy, Lucas Beyer, Alexander Kolesnikov, Dirk Weissenborn, Xiaohua Zhai, Thomas Unterthiner, Mostafa Dehghani, Matthias Minderer, Georg Heigold, Sylvain Gelly, Jakob Uszkoreit, and Neil Houlsby. An image is worth 16x16 words: Transformers for image recognition at scale. In *International Conference on Learning Representations*, 2021. URL <https://openreview.net/forum?id=YicbFdNTTy>.
- [17] Jonathan Frankle, Gintare Karolina Dziugaite, Daniel Roy, and Michael Carbin. Linear mode connectivity and the lottery ticket hypothesis. In *International Conference on Machine Learning*, pages 3259–3269. PMLR, 2020.

[18] Danilo Giampiccolo, Bernardo Magnini, Ido Dagan, and William B Dolan. The third pascal recognizing textual entailment challenge. In *Proceedings of the ACL-PASCAL workshop on textual entailment and paraphrasing*, pages 1–9, 2007.

[19] Gene H Golub and Charles F Van Loan. *Matrix computations*. JHU press, 2013.

[20] Almog Gueta, Elad Venezian, Colin Raffel, Noam Slonim, Yoav Katz, and Leshem Choshen. Knowledge is a region in weight space for fine-tuned language models. *arXiv preprint arXiv:2302.04863*, 2023.

[21] R Bar Haim, Ido Dagan, Bill Dolan, Lisa Ferro, Danilo Giampiccolo, Bernardo Magnini, and Idan Szpektor. The second pascal recognising textual entailment challenge. In *Proceedings of the Second PASCAL Challenges Workshop on Recognising Textual Entailment*, volume 7, pages 785–794, 2006.

[22] Peter Hase, Mohit Bansal, Been Kim, and Asma Ghandeharioun. Does localization inform editing? surprising differences in causality-based localization vs. knowledge editing in language models. *Advances in Neural Information Processing Systems*, 36, 2024.

[23] Tianxing He, Jun Liu, Kyunghyun Cho, Myle Ott, Bing Liu, James Glass, and Fuchun Peng. Analyzing the forgetting problem in pretrain-finetuning of open-domain dialogue response models. In *Proceedings of the 16th Conference of the European Chapter of the Association for Computational Linguistics: Main Volume*, pages 1121–1133, 2021.

[24] Yifei He, Shiji Zhou, Guojun Zhang, Hyokun Yun, Yi Xu, Belinda Zeng, Trishul Chilimbi, and Han Zhao. Robust multi-task learning with excess risks. In *Proceedings of the 41st International Conference on Machine Learning*, volume 235 of *Proceedings of Machine Learning Research*, pages 18094–18114. PMLR, 21–27 Jul 2024. URL <https://proceedings.mlr.press/v235/he24n.html>.

[25] Patrick Helber, Benjamin Bischke, Andreas Dengel, and Damian Borth. Eurosat: A novel dataset and deep learning benchmark for land use and land cover classification. *IEEE Journal of Selected Topics in Applied Earth Observations and Remote Sensing*, 12(7):2217–2226, 2019.

[26] Dan Hendrycks, Collin Burns, Steven Basart, Andy Zou, Mantas Mazeika, Dawn Song, and Jacob Steinhardt. Measuring massive multitask language understanding. *Proceedings of the International Conference on Learning Representations (ICLR)*, 2021.

[27] Torsten Hoefler, Dan Alistarh, Tal Ben-Nun, Nikoli Dryden, and Alexandra Peste. Sparsity in deep learning: Pruning and growth for efficient inference and training in neural networks. *Journal of Machine Learning Research*, 22(241):1–124, 2021.

[28] Minqing Hu and Bing Liu. Mining and summarizing customer reviews. In *Proceedings of the tenth ACM SIGKDD international conference on Knowledge discovery and data mining*, pages 168–177, 2004.

[29] Yuzheng Hu, Ruicheng Xian, Qilong Wu, Qiuling Fan, Lang Yin, and Han Zhao. Revisiting scalarization in multi-task learning: A theoretical perspective. *Advances in Neural Information Processing Systems*, 36, 2024.

[30] Gabriel Ilharco, Marco Tulio Ribeiro, Mitchell Wortsman, Ludwig Schmidt, Hannaneh Hajishirzi, and Ali Farhadi. Editing models with task arithmetic. In *The Eleventh International Conference on Learning Representations*, 2023. URL <https://openreview.net/forum?id=6t0Kwf8-jrj>.

[31] Shankar Iyer, Nikhil Dandekar, and Kornél Csernai. First quora dataset release: Question pairs. URL <https://quoradata.quora.com/First-Quora-Dataset-Release-Question-Pairs>.

[32] Xisen Jin, Xiang Ren, Daniel Preotiuc-Pietro, and Pengxiang Cheng. Dataless knowledge fusion by merging weights of language models. *arXiv preprint arXiv:2212.09849*, 2022.

[33] Jonathan Krause, Michael Stark, Jia Deng, and Li Fei-Fei. 3d object representations for fine-grained categorization. In *Proceedings of the IEEE international conference on computer vision workshops*, pages 554–561, 2013.

[34] Yann LeCun, Corinna Cortes, Chris Burges, et al. Mnist handwritten digit database, 2010.

[35] Namhoon Lee, Thalaiyasingam Ajanthan, and Philip HS Torr. Snip: Single-shot network pruning based on connection sensitivity. *arXiv preprint arXiv:1810.02340*, 2018.

[36] Stephanie Lin, Jacob Hilton, and Owain Evans. Truthfulqa: Measuring how models mimic human falsehoods. *arXiv preprint arXiv:2109.07958*, 2021.

[37] Bo Liu, Xingchao Liu, Xiaojie Jin, Peter Stone, and Qiang Liu. Conflict-averse gradient descent for multi-task learning. *Advances in Neural Information Processing Systems*, 34:18878–18890, 2021.

[38] Yinhan Liu, Myle Ott, Naman Goyal, Jingfei Du, Mandar Joshi, Danqi Chen, Omer Levy, Mike Lewis, Luke Zettlemoyer, and Veselin Stoyanov. Roberta: A robustly optimized bert pretraining approach. *arXiv preprint arXiv:1907.11692*, 2019.

[39] Yun Luo, Zhen Yang, Xuefeng Bai, Fandong Meng, Jie Zhou, and Yue Zhang. Investigating forgetting in pre-trained representations through continual learning. *arXiv preprint arXiv:2305.05968*, 2023.

[40] Michael S Matena and Colin A Raffel. Merging models with fisher-weighted averaging. *Advances in Neural Information Processing Systems*, 35:17703–17716, 2022.

[41] Yuval Netzer, Tao Wang, Adam Coates, Alessandro Bissacco, Baolin Wu, Andrew Y Ng, et al. Reading digits in natural images with unsupervised feature learning. In *NIPS workshop on deep learning and unsupervised feature learning*, volume 2011, page 7. Granada, Spain, 2011.

[42] Guillermo Ortiz-Jimenez, Alessandro Favero, and Pascal Frossard. Task arithmetic in the tangent space: Improved editing of pre-trained models. *Advances in Neural Information Processing Systems*, 36, 2024.

[43] Bo Pang and Lillian Lee. A sentimental education: Sentiment analysis using subjectivity summarization based on minimum cuts. *arXiv preprint cs/0409058*, 2004.

[44] Bo Pang and Lillian Lee. Seeing stars: Exploiting class relationships for sentiment categorization with respect to rating scales. *arXiv preprint cs/0506075*, 2005.

[45] Abhishek Panigrahi, Nikunj Saunshi, Haoyu Zhao, and Sanjeev Arora. Task-specific skill localization in fine-tuned language models. In Andreas Krause, Emma Brunskill, Kyunghyun Cho, Barbara Engelhardt, Sivan Sabato, and Jonathan Scarlett, editors, *Proceedings of the 40th International Conference on Machine Learning*, volume 202 of *Proceedings of Machine Learning Research*, pages 27011–27033. PMLR, 23–29 Jul 2023. URL <https://proceedings.mlr.press/v202/panigrahi23a.html>.

[46] Judea Pearl. Direct and indirect effects. In *Probabilistic and causal inference: the works of Judea Pearl*, pages 373–392. 2022.

[47] Sergio Pissanetzky. *Sparse matrix technology-electronic edition*. Academic Press, 1984.

[48] Alec Radford, Jeff Wu, Rewon Child, David Luan, Dario Amodei, and Ilya Sutskever. Language models are unsupervised multitask learners. 2019.

[49] Alec Radford, Jong Wook Kim, Chris Hallacy, Aditya Ramesh, Gabriel Goh, Sandhini Agarwal, Girish Sastry, Amanda Askell, Pamela Mishkin, Jack Clark, et al. Learning transferable visual models from natural language supervision. In *International conference on machine learning*, pages 8748–8763. PMLR, 2021.

[50] Colin Raffel, Noam Shazeer, Adam Roberts, Katherine Lee, Sharan Narang, Michael Matena, Yanqi Zhou, Wei Li, and Peter J Liu. Exploring the limits of transfer learning with a unified text-to-text transformer. *Journal of machine learning research*, 21(140):1–67, 2020.

[51] Pranav Rajpurkar, Jian Zhang, Konstantin Lopyrev, and Percy Liang. Squad: 100,000+ questions for machine comprehension of text. *arXiv preprint arXiv:1606.05250*, 2016.

[52] Richard Socher, Alex Perelygin, Jean Wu, Jason Chuang, Christopher D Manning, Andrew Y Ng, and Christopher Potts. Recursive deep models for semantic compositionality over a sentiment treebank. In *Proceedings of the 2013 conference on empirical methods in natural language processing*, pages 1631–1642, 2013.

[53] Johannes Stallkamp, Marc Schlipsing, Jan Salmen, and Christian Igel. The german traffic sign recognition benchmark: a multi-class classification competition. In *The 2011 international joint conference on neural networks*, pages 1453–1460. IEEE, 2011.

[54] Mingjie Sun, Zhuang Liu, Anna Bair, and J Zico Kolter. A simple and effective pruning approach for large language models. *arXiv preprint arXiv:2306.11695*, 2023.

[55] Mukund Sundararajan, Ankur Taly, and Qiqi Yan. Axiomatic attribution for deep networks. In *International conference on machine learning*, pages 3319–3328. PMLR, 2017.

[56] Rohan Taori, Ishaan Gulrajani, Tianyi Zhang, Yann Dubois, Xuechen Li, Carlos Guestrin, Percy Liang, and Tatsunori B. Hashimoto. Stanford alpaca: An instruction-following llama model. https://github.com/tatsu-lab/stanford_alpaca, 2023.

[57] Jesse Vig, Sebastian Gehrmann, Yonatan Belinkov, Sharon Qian, Daniel Nevo, Yaron Singer, and Stuart Shieber. Investigating gender bias in language models using causal mediation analysis. *Advances in neural information processing systems*, 33:12388–12401, 2020.

[58] Ellen M Voorhees et al. The trec-8 question answering track report. In *Trec*, volume 99, pages 77–82, 1999.

[59] Alex Wang, Amanpreet Singh, Julian Michael, Felix Hill, Omer Levy, and Samuel R Bowman. Glue: A multi-task benchmark and analysis platform for natural language understanding. *arXiv preprint arXiv:1804.07461*, 2018.

[60] Ke Wang, Nikolaos Dimitriadis, Guillermo Ortiz-Jimenez, François Fleuret, and Pascal Frossard. Localizing task information for improved model merging and compression. In *Forty-first International Conference on Machine Learning*, 2024.

[61] Janyce Wiebe, Theresa Wilson, and Claire Cardie. Annotating expressions of opinions and emotions in language. *Language resources and evaluation*, 39:165–210, 2005.

[62] Adina Williams, Nikita Nangia, and Samuel R Bowman. A broad-coverage challenge corpus for sentence understanding through inference. *arXiv preprint arXiv:1704.05426*, 2017.

[63] Thomas Wolf, Lysandre Debut, Victor Sanh, Julien Chaumond, Clement Delangue, Anthony Moi, Pierric Cistac, Tim Rault, Rémi Louf, Morgan Funtowicz, et al. Transformers: State-of-the-art natural language processing. In *Proceedings of the 2020 conference on empirical methods in natural language processing: system demonstrations*, pages 38–45, 2020.

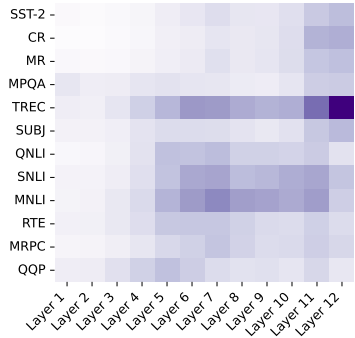
[64] Mitchell Wortsman, Gabriel Ilharco, Samir Ya Gadre, Rebecca Roelofs, Raphael Gontijo-Lopes, Ari S Morcos, Hongseok Namkoong, Ali Farhadi, Yair Carmon, Simon Kornblith, et al. Model soups: averaging weights of multiple fine-tuned models improves accuracy without increasing inference time. In *International conference on machine learning*, pages 23965–23998. PMLR, 2022.

[65] Mitchell Wortsman, Gabriel Ilharco, Jong Wook Kim, Mike Li, Simon Kornblith, Rebecca Roelofs, Raphael Gontijo Lopes, Hannaneh Hajishirzi, Ali Farhadi, Hongseok Namkoong, et al. Robust fine-tuning of zero-shot models. In *Proceedings of the IEEE/CVF conference on computer vision and pattern recognition*, pages 7959–7971, 2022.

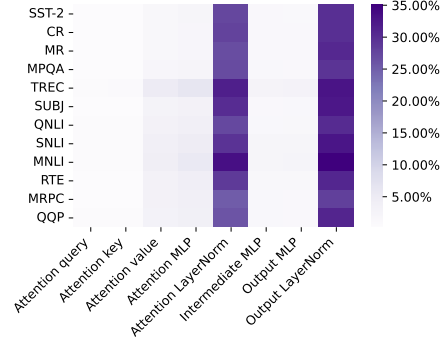
[66] Jianxiong Xiao, Krista A Ehinger, James Hays, Antonio Torralba, and Aude Oliva. Sun database: Exploring a large collection of scene categories. *International Journal of Computer Vision*, 119:3–22, 2016.

- [67] Prateek Yadav, Derek Tam, Leshem Choshen, Colin Raffel, and Mohit Bansal. TIES-merging: Resolving interference when merging models. In *Thirty-seventh Conference on Neural Information Processing Systems*, 2023. URL <https://openreview.net/forum?id=xtaX3WyCj1>.
- [68] Enneng Yang, Zhenyi Wang, Li Shen, Shiwei Liu, Guibing Guo, Xingwei Wang, and Dacheng Tao. Adamerging: Adaptive model merging for multi-task learning. *arXiv preprint arXiv:2310.02575*, 2023.
- [69] Zhilin Yang, Peng Qi, Saizheng Zhang, Yoshua Bengio, William W Cohen, Ruslan Salakhutdinov, and Christopher D Manning. Hotpotqa: A dataset for diverse, explainable multi-hop question answering. *arXiv preprint arXiv:1809.09600*, 2018.
- [70] Le Yu, Bowen Yu, Haiyang Yu, Fei Huang, and Yongbin Li. Language models are super mario: Absorbing abilities from homologous models as a free lunch. *arXiv preprint arXiv:2311.03099*, 2023.
- [71] Tianhe Yu, Saurabh Kumar, Abhishek Gupta, Sergey Levine, Karol Hausman, and Chelsea Finn. Gradient surgery for multi-task learning. *Advances in Neural Information Processing Systems*, 33:5824–5836, 2020.
- [72] Yu Zhang and Qiang Yang. A survey on multi-task learning. *IEEE Transactions on Knowledge and Data Engineering*, 34(12):5586–5609, 2021.

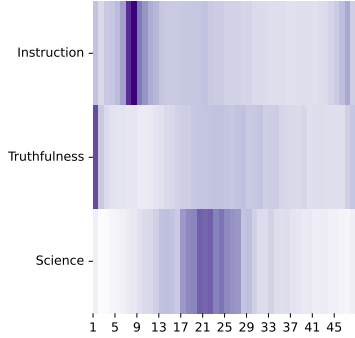
A More experiments



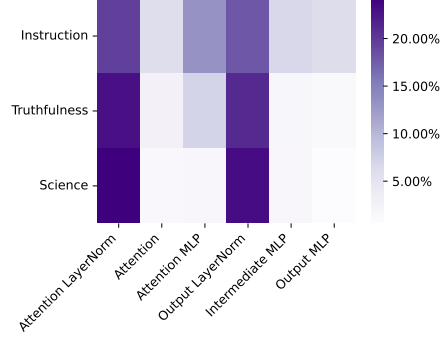
(a) Distribution of localized regions in different network layers for language tasks in the RoBERTa-base model.



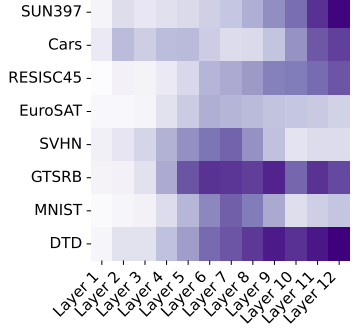
(b) Distribution of localized regions in different network components for language tasks in the RoBERTa-base model.



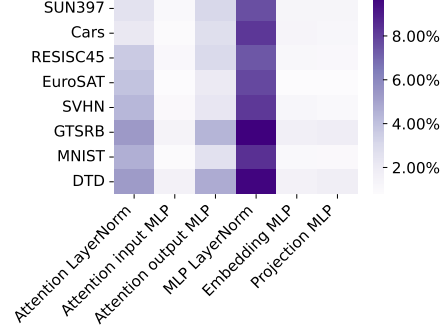
(c) Distribution of localized regions in different network layers for language tasks in the GPT2-XL model.



(d) Distribution of localized regions in different network components for language tasks in the GPT2-XL model.



(e) Distribution of localized regions in different network layers for vision tasks.



(f) Distribution of localized regions in different network components for vision tasks.

Figure 9: The localized regions are predominantly found in the LayerNorm parameters, while different tasks are associated with different layers. The percentages represent the proportion of localized parameters in each component.

Where are the localized regions? We analyze the distribution of the localized regions for both language and vision tasks in Figure 9, both in terms of the layer index and the transformer components. For the layers, different tasks seem to occupy different layers, although the earlier layers in the network seldomly appear in the localized regions. Interestingly, most of the localized regions concentrate in the LayerNorm parameters. This pattern can possibly be attributed to a covariate shift observed in

the finetuning data compared to the pretraining data, necessitating adjustments to the LayerNorm parameters to accommodate this shift.

Table 5: Single-task grafted performance of RoBERTa-base models on twelve NLP tasks.

Task	SST-2	CR	MR	MPQA	TREC	SUBJ	QNLI	SNLI	MNLI	RTE	MRPC	QQP	Average
Single-task finetuned	0.898	0.894	0.844	0.848	0.938	0.931	0.764	0.791	0.706	0.643	0.766	0.716	0.811
Single-task grafted	0.897	0.883	0.855	0.844	0.918	0.933	0.751	0.772	0.703	0.639	0.745	0.708	0.804
Recovered proportion	0.999	0.988	1.013	0.995	0.979	1.002	0.983	0.976	0.996	0.994	0.973	0.989	0.991

Table 6: Single-task grafted performance of GPT2-XL models on three NLP tasks.

Task	MMLU	TruthfulQA	ARC	Average
Single-task finetuned	0.273	0.488	0.472	0.411
Single-task grafted	0.264	0.436	0.475	0.392
Recovered proportion	0.969	0.893	1.007	0.953

Table 7: Single-task grafted performance of CLIP ViT-B/32 models on eight vision tasks.

Task	SUN397	Cars	RESISC45	EuroSAT	SVHN	GTSRB	MNIST	DTD	Average
Single-task finetuned	0.753	0.777	0.961	0.997	0.975	0.987	0.997	0.794	0.905
Single-task grafted	0.731	0.772	0.955	0.989	0.963	0.973	0.996	0.781	0.895
Recovered proportion	0.970	0.993	0.994	0.992	0.988	0.985	0.999	0.983	0.989

Full grafted performance. We evaluate the quality of the localized regions by the grafted performance. For the i -th task, we only add up the localized regions in the task vectors back to the pretrained model, i.e., $\theta_{\text{pre}} + \gamma_i \odot \tau_i$. The results with a localization region of 1% is shown in Tables 5 to 7. For almost all tasks, using only the tiny localized region recovers nearly 99% of the finetuned performance. For GPT2-XL, the performance is slightly worse because we cannot use the evaluation data for the localization step. However, the results are still strong even with surrogate datasets with similar purposes, demonstrating the flexibility and robustness of our algorithm. Overall, this shows that our localization approach is effective in locating regions containing essential skills acquired during finetuning, and the localized regions can be viewed as compact representations of the finetuned models.

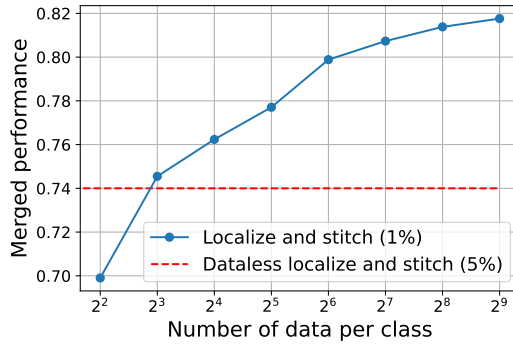


Figure 10: Merged performance versus available data in vision tasks.

Effect of data availability. Similar to Figure 7, we plot the same trend of our method across various data availability scenarios with a localization regions of 1% on the vision tasks as well (Figure 10). We can still see the clear pattern that the performance monotonically increases with more data available, and does not show saturation even with 512-shot data. In addition, with 8-shot data, the performance of localization improves over the dataless version, the same observation as in language tasks.

Runtime. We compare the runtime of Localize-and-Stitch and other baselines. We divide the algorithms into two categories: dataless and requiring data. Note that task arithmetic and TIES-Merging can fall in both categories, with the difference of whether performing hyperparameter tuning (scaling factor α for both, and sparsity for TIES). For the hyperparameter tuning, we follow

Table 8: Runtime for dataless algorithms.

Method	Runtime (s)
Simple averaging	189.17
Task arithmetic	186.32
TIES-Merging	350.47
Dataless Localize-and-Stitch	304.85

Table 9: Runtime for algorithms requiring data.

Method	Runtime (s)
Fisher Merging	293.33
Task arithmetic (tuned)	6562.14
TIES-Merging (tuned)	24042.43
RegMean	22987.54
AdaMerging	81326.57
Localize-and-Stitch	5130.05

the common practice in [30, 67] to grid search over $\{0.1, 0.2 \dots, 0.9\}$ for the scaling factor and $\{0.1, 0.2, 0.3\}$ for the sparsity.

We report the runtime in Tables 8 and 9 for merging twelve NLP tasks with RoBERTa-base. For the dataless algorithms, simple averaging and task arithmetic are very efficient, as they only involve arithmetic operations on the weights. Both TIES and our dataless version requires sorting the task vectors to get the top- $k\%$ largest elements, so the runtime is slower. Compared with TIES, we do not have the step for resolving sign conflicts, so it takes less time. For algorithms requiring data, Fisher merging is the most efficient, as it uses a diagonal estimate of the Fisher information matrices with little data (256 per task). Both task arithmetic and TIES-Merging show substantial time increase, as they need to do grid search on 9 and 27 hyperparameters respectively as well as evaluating on the validation data in each run. AdaMerging takes significantly more runtime to execute compared with others, and the reason could be that entropy minimization converges slowly, as we observe that AdaMerging requires around 500 epochs to converge. Compared with other algorithms, Localize-and-Stitch executes in a relatively short amount of time, showing its effectiveness.

Table 10: Comparison of performance and efficiency for continual learning.

		SST-2+CR	+TREC	+SUBJ	+QNLI	+QQP
Task arithmetic	Average performance	0.907	0.864	0.853	0.817	0.762
	Runtime (s)	1340	1760	2183	2654	2970
TIES	Average performance	0.897	0.832	0.827	0.796	0.757
	Runtime (s)	3421	5031	6894	8147	9358
Localize-and-Stitch	Average performance	0.906	0.905	0.897	0.856	0.827
	Runtime (s)	806	421	403	462	455

Continual learning. As mentioned in Section 3.3, our approach is particularly efficient in the continual learning setting. To illustrate the efficiency, we start from merging the SST-2 and CR RoBERTa models, and incrementally add 4 more tasks to simulate a continual learning setting. The tasks are selected by representativeness (including sentiment analysis, sentence classification, NLI etc). We compare our method against two baselines: task arithmetic and TIES, with merging coefficients tuned across $\{0.0, 0.1, \dots, 0.9, 1.0\}$. The results from Table 10 demonstrate that: i) **Performance:** Localize-and-Stitch consistently outperforms the baselines, with the performance margin increasing as more tasks are involved, showing its ability to reduce task interference. ii) **Runtime:** The runtime for both TIES and task arithmetic increases with each added task due to the need for hyperparameter search from scratch and performance validations, while the runtime of Localize-and-Stitch generally remains constant, reflecting its efficiency in continual learning scenarios.

B Comparison between Dataless Localize-and-Stitch and TIES-Merging

Due to the similarity of the dataless version of our approach with TIES-Merging [67], we compare them in detail.

The first step of both algorithms is similar: select the top- $k\%$ largest positions in the task vector. The primary difference lies in the selection threshold: Dataless Localize-and-Stitch selects the top-5%, while TIES selects the top-20%. However, as shown in Section 3.1, we find that when a

Table 11: Comparison of Dataless Localize-and-Stitch and TIES on language tasks.

Task	SST-2	CR	MR	MPQA	TREC	SUBJ	QNLI	SNLI	MNLI	RTE	MRPC	QQP	Average
Dataless Localize-Stitch (5%)	0.909	0.907	0.864	0.821	0.462	0.762	0.558	0.690	0.618	0.688	0.837	0.693	0.734
TIES (5%)	0.858	0.837	0.822	0.712	0.142	0.290	0.467	0.191	0.271	0.438	0.743	0.358	0.510
TIES (20%)	0.805	0.805	0.728	0.791	0.226	0.549	0.552	0.501	0.379	0.477	0.816	0.572	0.600

Table 12: Comparison of Dataless Localize-and-Stitch and TIES on vision tasks.

Task	SUN397	Cars	RESISC45	EuroSAT	SVHN	GTSRB	MNIST	DTD	Average
Dataless Localize-Stitch (5%)	0.669	0.647	0.768	0.746	0.817	0.726	0.973	0.576	0.740
TIES (5%)	0.520	0.552	0.669	0.683	0.874	0.606	0.982	0.480	0.671
TIES (20%)	0.598	0.586	0.707	0.797	0.862	0.721	0.983	0.542	0.725

localized region already contains sufficient task-specific knowledge, including more parameters only introduces more task interference. This observation could partially explain our superior performance. However, this is not the only limitation in TIES, as reducing the threshold in TIES to be 5% does not yield an improved performance as demonstrated in Tables 11 and 12.

In the subsequent merging step, Dataless Localize-and-Stitch can be viewed as a simplified version of TIES. When dealing with overlap for the localized regions, Dataless Localize-and-Stitch simply averages the parameters in these overlapping area. On the other hand, TIES first sums positive and negative parameters separately at each overlapping position, and determines the dominant sign based on their total magnitudes, a process akin to a weighted majority vote. Then, TIES only keep the parameter values that aligns with the elected sign, and compute the mean.

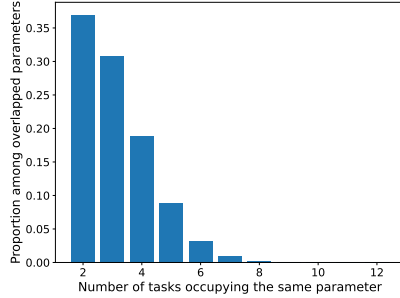


Figure 11: When merging 12 NLP tasks with top-20% selection in TIES, most overlapping regions only involve 2 or 3 tasks. This is the regime where the sign election process in TIES is less effective in.

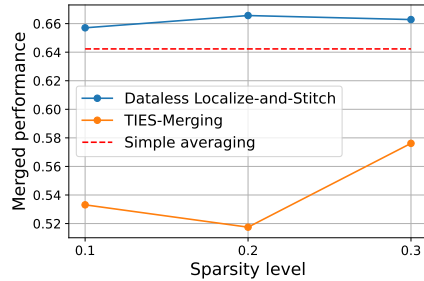


Figure 12: When dealing with two conflicting tasks, the sign election stage of TIES is not effective. The performance of TIES is consistently worse than simple averaging on all parameters.

This approach by TIES might be more advantageous when overlapping regions involve a larger number of tasks. The rationale is that with more tasks contributing to an overlap, the process of sign determination and selective averaging may more accurately capture the consensus of task vectors for all tasks as a whole. However, when only two tasks are involved (which is often the case as shown in Figure 11), TIES may only retain parameters predominantly from the task with the larger magnitude at each position. In such scenarios, important parameters for both tasks could be alternately ignored, potentially degrading performance for both tasks. This selective process might, therefore, impair the overall efficacy in maintaining crucial task-specific information, particularly in tightly contested regions. We demonstrate this in Figure 12, where we use the same example of conflicting tasks as in Section 3.1, i.e., QNLI and MNLI. When merging models on two conflicting tasks, the performance of TIES is significantly worse than simple averaging on all model parameters across all sparsity levels.

C Details on localization

Here, we detail the skill attribution method in [45] and explain the difference with our formulation. Panigrahi et al. [45] aims to localize task-specific skills contained in finetuned language models. They introduce model grafting, where for given pretrained and finetuned model parameters θ_{pre} and θ_{ft} ,

they graft parameters of θ_{ft} in the region γ onto the pretrained model as

$$\overline{\theta_{\text{ft}}}(\gamma) = \gamma \odot \theta_{\text{ft}} + (1 - \gamma) \odot \theta_{\text{pre}}.$$

With the grafting operation, they find the localized region with the following optimization procedure, where they essentially find the region leading to the best grafted performance.

$$\operatorname{argmin}_{\gamma \in \{0,1\}^d: \|\gamma\|_0 \leq s} \ell_{\tau}(\gamma \odot \theta_{\text{ft}} + (1 - \gamma) \odot \theta_{\text{pre}})$$

They also use a reparametrization of the binary mask γ as the sigmoid of a real-valued vector S , and reformulate the problem as

$$\begin{aligned} & \operatorname{argmin}_{S \in \mathbb{R}^d} \ell_i(\gamma \odot \theta_{\text{ft}} + (1 - \gamma) \odot \theta_{\text{pre}}), \\ & \gamma := \gamma_{\text{base}} \odot (1 - \sigma(S)) + (1 - \gamma_{\text{base}}) \odot \sigma(S), \end{aligned} \quad (2)$$

where γ_{base} is the top- $k\%$ largest elements in the task vector. This serves as an initialization for the optimization. In comparison, our formulation is as follows

$$S_i = \operatorname{argmin}_{S \in \mathbb{R}^d} \ell_i(\theta_{\text{pre}} + \sigma(S) \odot \tau_i) + \lambda \|\sigma(S)\|_1,$$

There are two main differences between the formulations. Firstly, our formulation of S is more straightforward, as we directly have $\gamma = \sigma(S)$. In contrast, S in Equation (2) serves as a selector of whether to take the value from γ_{base} , leading to more complex computation. Secondly, our approach uses the L_1 constraint to control the sparsity in a more fine-grained manner, while Equation (2) does not have this constraint, and the authors control the sparsity via early stopping.

Table 13: Comparison of localization methods on RoBERTa-base models on twelve language tasks.

Task	SST-2	CR	MR	MPQA	TREC	SUBJ	QNLI	SNLI	MNLI	RTE	MRPC	QQP	Average
Single-task finetuned	0.898	0.894	0.844	0.848	0.938	0.931	0.764	0.791	0.706	0.643	0.766	0.716	0.811
Single-task grafted (Ours)	0.897	0.883	0.855	0.844	0.918	0.933	0.751	0.772	0.703	0.639	0.745	0.708	0.804
Single-task grafted [45]	0.902	0.908	0.862	0.851	0.884	0.925	0.752	0.756	0.676	0.643	0.757	0.693	0.801
Merged (Ours)	0.896	0.896	0.849	0.828	0.782	0.820	0.734	0.621	0.580	0.633	0.820	0.651	0.759
Merged [45]	0.897	0.895	0.847	0.831	0.816	0.803	0.727	0.649	0.580	0.633	0.819	0.656	0.763

Table 14: Comparison of localization methods on CLIP ViT-B/32 models on eight vision tasks.

Task	SUN397	Cars	RESISC45	EuroSAT	SVHN	GTSRB	MNIST	DTD	Average
Single-task finetuned	0.753	0.777	0.961	0.997	0.975	0.987	0.997	0.794	0.905
Single-task grafted (Ours)	0.731	0.772	0.955	0.989	0.963	0.973	0.996	0.781	0.895
Single-task grafted [45]	0.731	0.750	0.935	0.959	0.929	0.932	0.976	0.753	0.871
Merged (Ours)	0.672	0.683	0.818	0.894	0.879	0.866	0.948	0.629	0.799
Merged [45]	0.669	0.678	0.798	0.861	0.846	0.826	0.919	0.653	0.781

We present the performance comparison of the two localization methods in Tables 13 and 14. In both cases, our approach with Equation (1) outperforms [45]. The performance may come from the fact that [45] use early stopping to control the sparsity, which results in incomplete optimization for the masks. We also report the merged performance by following the same stitching process. On the language tasks, the performance is similar, while on the vision tasks, our localization leads to better merged performance.

D GPT2-XL experiment details

For the experiments in Section 4.2, we use the following three checkpoints from Hugging Face:

- Locutusque/gpt2-large-conversational
- Onlydrinkwater/gpt2xl_language_math_520_10base
- Rachneet/gpt2-xl-alpaca

They are all finetuned on the original release of the GPT2-XL model `openai-community/gpt2-xl`. The selection of the three models and associated tasks is a result of an extensive evaluation process. After testing dozens of finetuned GPT-2XL checkpoints, we establish specific criteria to ensure the relevance and rigor of our experiments: The checkpoints should

- be fully finetuned instead of PEFT,
- have a well-defined and evaluable downstream task,
- perform noticeably better than the pretrained model on its respective task.

We find that most finetuned checkpoints do not meet the last criterion, which is crucial for substantiating the benefits of our merging method. Consequently, the three models and tasks combinations chosen best satisfy all three criteria, making them the most appropriate for our purposes.

E Datasets

Vision datasets Following the practice in [30], we use the following 8 datasets for the vision part of our experiments:

- SUN397 [66]. The Scene Understanding dataset contains 108,754 images of 397 classes.
- Stanford Cars [33]. The Stanford Cars dataset contains 16,185 images of 196 classes of cars.
- RESISC45 [6]. The REmote Sensing Image Scene Classification dataset contains 31,500 images, covering 45 scene classes.
- EuroSAT [25]. The EuroSAT dataset consists of 10 classes with 27000 labeled and geo-referenced samples. Each class represents a different land use and land cover.
- SVHN [41]. The Street View House Numbers dataset contains 600,000 digit images in 10 classes of printed digits cropped from pictures of house number plates.
- GTRSB [53]. The German Traffic Sign Recognition Benchmark contains 43 classes of traffic signs with more than 50,000 images.
- MNIST [34]. The MNIST dataset contains 60,000 training images and 10,000 testing images of 10 handwritten digits.
- DTD [8]. The Describable Texture Dataset contains 5,640 texture images in the wild with 47 classes.

SUN397, RESISC45 and DTD are under the Creative Commons Attribution-ShareAlike 4.0 International License. Stanford Cars is under the ImageNet License. EuroSAT is under MIT License. MNIST is under Gnu General Public License. GTRSB and SVHN are under CCBY-SA License.

Language datasets Following the practice in [45], we use the following 12 datasets for the language part of our experiments. The majority comes from the GLUE benchmark [59].

- SST-2 [52]. The Stanford Sentiment Treebank is a sentiment analysis dataset, which contains sentences from movie reviews and human annotated binary sentiments.
- CR [28]. The Customer Review dataset consists of customer reviews on e-commerce products with binary sentiment labels.
- MR [44]. The Movie Review dataset consists of movie reviews with binary sentiment labels.
- MPQA [61]. The Multi-Perspective Question Answering dataset contains news articles and text documents manually annotated for opinions and other private states including beliefs, emotions, sentiments, etc. Here, we use it for binary sentiment classification.
- TREC [58]. The Text REtrieval Conference (TREC) dataset contains 6k questions phrased by users and categorized into a small number of categories. The task is to classify the questions into these categories.
- SUBJ [43]. The SUBJjectivity dataset contains 10k movie reviews with an annotation of whether the review describes something subjective or objective about the movie.

- QNLI [59]. The Question-answering NLI dataset is converted from the Stanford Question Answering Dataset (SQuAD) [51], which contains questions and the paragraphs that contain the answer to the corresponding questions. QNLI converts SQuAD into sentence pair classification by forming a pair between each question and each sentence in the corresponding context, where the task is to predict whether the context contains the answer to the question.
- SNLI [2]. The Stanford Natural Language Inference dataset contains 570k sentence pairs manually labeled as entailment, contradiction or neutral.
- MNLI [62]. The Multi-Genre Natural Language Inference Corpus is a collection of 433k sentence pairs annotated with textual entailment information.
- RTE [59]. The Recognizing Textual Entailment dataset contains a series of textual entailment challenges, including RTE1 [11], RTE2 [21], RTE3 [18] and RTE5 [1]. The neutral and contradiction classes are combined into a no entailment class.
- MRPC [15]. The Microsoft Research Paraphrase Corpus consists of sentence pairs from online news sources, with human annotations of whether the sentences in the pair are semantically equivalent. Since the classes are imbalanced, we report the F1 score.
- QQP [31]. The Quora Question Pairs dataset consists of question-answer pairs from the website Quora. The task is to determine whether two questions are semantically equivalent.

CR, RTE, MRPC, QQP, QNLI are under CCBY-SA License. MRPC is under Microsoft Research License. MNLI is under OANC’s License. SNLI is under a Creative Commons Attribution-ShareAlike 4.0 International License.

GPT datasets We introduce the datasets used for GPT2-XL experiments.

- MMLU [26]. The Massive Multitask Language Understanding measures knowledge in 57 subjects across STEM, humanities, social science, etc.
- ARC [9]. The AI2 Reasoning Challenge dataset contains 7,787 grade-school level, multiple choice science questions.
- TruthfulQA [36]. The TruthfulQA dataset measure whether a model is truthful in generating answers to questions. It comprises 817 questions spanning 38 categories, including health, law, finance, etc.
- Alpaca [56]. The Alpaca dataset contains 52,000 instruction-following examples.
- GSM8k [10]. The Grade School Math 8K dataset contains 8,500 high quality grade school math problems created by human problem writers. The problems take 2 to 8 steps to solve.
- HotpotQA [69]. The HotpotQA dataset is a question answering dataset featuring multi-hop questions.

ARC is under CC BY-SA License. TruthfulQA and Alpaca are under Apache License 2.0. MMLU and GSM8k are under MIT License. HotpotQA is under CC BY-SA 4.0 License.

F Implementation details

The experiments are run on NVIDIA RTX A6000 GPUs with 48GB memory.

Finetuning. For the experiments on RoBERTa-base, we perform the finetuning process following the same procedure as [45]. Specifically, we use a batch size of 4 and a learning rate of 2e-5 to finetune on each of the language tasks for 10 epochs with the SGD optimizer. For the experiments on CLIP ViT, we directly use the finetuned checkpoints provided in [30] with the data preprocessing step provided in [68]. The finetuned models in the GPT2-XL experiments in provided in Appendix D.

Localization. Following the practice in [45], in the localization step, we initialize the trainable real-valued vector S as the mask for top- $k\%$ largest entries in the task vector. Since the actual map is rounded from $\sigma(S)$ but not S , we choose the initial values of S to be either 0 or 3, as $\sigma(3)$ is sufficiently close to 1. To achieve a sparsity level of 1%, we use the learning rate 1e7, batch size 16, L_1 regularization factor λ 1e-5 and perform the optimization for 10 epochs on 64-shot data from each task. Following common practice in [45, 67], we only perform localization in the transformer blocks, and do not consider embedding layers.

Baselines. We use both task arithmetic and TIES-Merging in a dataless manner, meaning that we directly use their recommended hyperparameters without tuning it. To be specific, for task arithmetic, the recommended scaling factor is 0.4. For TIES-Merging, the recommended scaling factor is 1 and sparsity level is 20%. This ensures a fair comparison with `Dataless Localize-and-Stitch`, which we also apply a fixed sparsity level across all experiments, namely 5%.

G Limitations

Our work shares some limitations with existing model merging methods. Firstly, the applicability of our method is limited to merging models finetuned from the same initialization. Secondly, although in Section 3.1, we provide empirical findings that support our motivations, it remains unclear whether the arguments can be tested theoretically. In fact, the theoretical understanding of the effectiveness of model merging is still underexplored, only with the few attempts from linear mode connectivity [17] and tangent task spaces [42]. Thirdly, although the conflicts among tasks can be significantly reduced with our approach, the performance still lags behind the single-task finetuned models. This phenomenon calls for more understanding of the difficulties in model merging beyond task conflicts.